Biol Cybern (2008) 98:185–194
DOI 10.1007/s00422-007-0208-7

ORIGINAL PAPER

Biological Cybernetics

Spike-timing in primary sensory neurons: a model of somatosensory transduction in the rat

Ben Mitchinson · Ehsan Arabzadeh · Mathew E. Diamond · Tony J. Prescott

Received: 30 March 2006 / Accepted: 28 October 2007 / Published online: 5 January 2008

Abstract In previous work, we constructed a simple electromechanical model of transduction in the rat mystacial follicle that was able to replicate primary afferent response profiles to a variety of whisker deflection stimuli. Here, we update that model to fit newly available spike-timing response data, and demonstrate that the new model produces appropriate responses to richer stimuli, including pseudo white noise and natural textures, at a spike-timing level of detail. Additionally, we demonstrate reliable distributed encoding of multi-component oscillatory signals. No modifications were necessary to the mechanical model of the physical components of the follicle–sinus complex, supporting its generality. We conclude that this model, and its continued development, will aid the understanding both of somatosensory systems in general, and of physiological results from higher (e.g. thalamocortical) systems by accurately characterising the signals on which they operate.

1 Introduction

The rat (amongst other mammals) enjoys an impressively acute tactile sensory modality, the sensors of which include large mobile whiskers on either side of the snout (mystacial macrovibrissae, Fig. 1) (Waite 2004; Kleinfeld et al. 2006). The whisker system is considered a particularly accessible model of sensory systems in general, mainly for its unique discrete anatomical organisation, with each whisker represented as a cellular aggregate in several nuclei at all levels of the neuraxis, but also for the controllability and repeatability of whisker-applied stimuli (Woolsey and Van der Loos 1970; Van der Loos 1976; Ma 1991; Ahissar et al. 2000; Pinto et al. 2000; Mehta and Kleinfeld 2004). The peripheral parts of the system are (a) the whiskers themselves, each housed in (b) a specialised hair follicle bearing a few hundred mechanoreceptors, which, more centrally, become (c) a primary afferent nerve, which projects to (d) the trigeminal sensory complex in brainstem. Here, after the first level of synaptic integration, information is passed on to many other nuclei at all levels of the brain (Waite 2004). A complete and accurate characterisation of the signal transduction performed between a and c, then, will facilitate study of these other nuclei and their associated sensorimotor loops, whilst revealing insights which we expect to be applicable to somatosensory systems in general.

To this end, many studies have measured aspects of transduction in the whisker-follicle-afferent subsystem, usually using computer-controlled ramp-and-hold whisker deflection stimuli, and recording from primary afferent cells (Zucker and Welker 1969; Hahn 1971; Gottschaldt et al. 1973; Dykes 1975; Gottschaldt and Vahle-Hinz 1981; Gibson and Welker 1983a,b; Lichtenstein et al. 1990; Shoykhet et al. 2000; Szwed et al. 2003). These results are difficult to collate since experimental protocols vary and evolve. It is increasingly considered that parametric models can help in this regard, parsimoniously accounting for rich but sparse data, and modelling has been used previously to help marshal data from thalamocortical interactions (Rhodes and Llinás 2005), the whisker system in particular (Kyriazi and Simons 1993), and from other tactile transduction systems (Freeman and Johnson 1982; Slavík and Bell 1995; Bensmaïa 2002). We

B. Mitchinson (✉) · T. J. Prescott
Adaptive Behaviour Research Group, Department of Psychology, The University of Sheffield, Sheffield S10 2TP, UK
e-mail: b.mitchinson@shef.ac.uk

T. J. Prescott
e-mail: t.j.prescott@shef.ac.uk

E. Arabzadeh · M. E. Diamond
Cognitive Neuroscience Sector, Italian Institute of Technology—SISSA unit, International School for Advanced Studies, Trieste, Italy

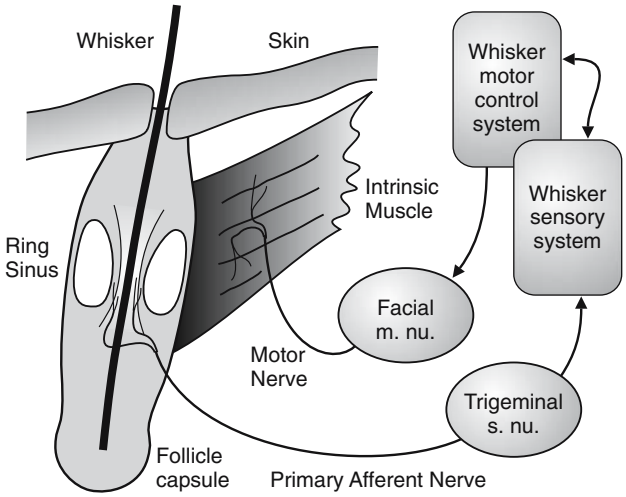

Fig. 1 Schematic of whisker-follicle assembly and connections to nervous system via trigeminal sensory and facial motor nuclei. The sensory and motor whisker systems are densely interconnected

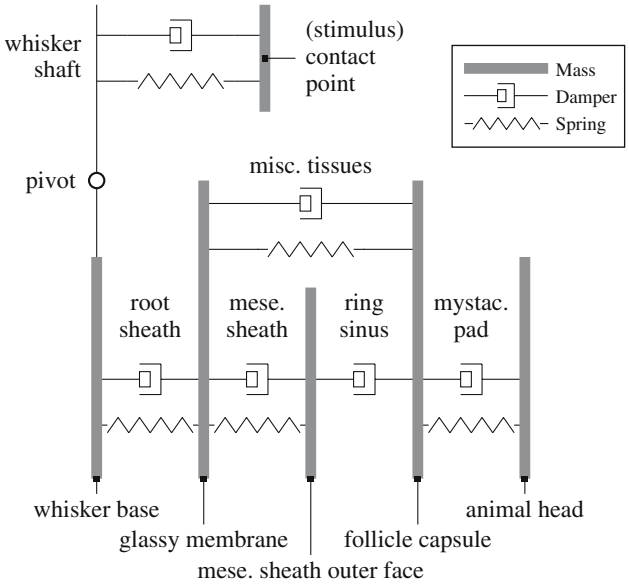

Fig. 2 Mechanical part of model. Masses/springs/dampers are represented iconically (see legend), the whisker shaft pivot point as a *circle*

previously reported the only existing model of mystacial transduction in rat (Mitchinson et al. 2004). This model was able to well reproduce the response envelopes of the two main categories of primary afferent (rapidly- and slowly-adapting, RA and SA) during simulated protocols of direct whisker deflection and fictive whisking against obstacles.

We wish to demonstrate that simple models can reproduce spike-timing data to test the hypothesis that first-order neuron responses could be governed by reasonably simple electro-mechanical models, even at this level of detail. Recent success in modelling of macaque monkey mechanoreceptors (Bensmaïa 2002; Bensmaïa et al. 2005) is encouraging in this regard. Recent work by Arabzadeh et al. (2005) has made spike-timing data available, and these indicate that at least some primary afferents express no apparent stimulus memory, but do express both absolute and relative refractory behaviour—these aspects of cell behaviour are theoretically realistic and easily modelled (Eliasmith and Anderson 2003) and have been used successfully in a previous transduction model (Slavík and Bell 1995); these are the modifications to the cell model introduced here. In the remainder of this section, we review the existing model and the new data.

The model consists of two parts, simulated mechanical and simulated electrical, both of which are simulated in discrete time with fixed integration sample rate f_S. The mechanical part has components representing the whisker shaft from stimulus contact point to base, and internal components of the follicle including the root and mesenchymal sheaths, the glassy membrane, the ring sinus and the follicle capsule (Rice et al. 1986; Ebara et al. 2002), Fig. 2. The two-dimensional position of each mass at sample n is denoted $\mathbf{s}_{i,n} = [s^1_{i,n}, s^2_{i,n}]$, with i the index from Table 1. The free motion of each mass

Table 1 Mechanical model parameters

Mass description	i	m	ij	k_{ij}	d_{ij}
Contact point	1	0.5	12	100	0.45
Whisker base	2	20	23	20	1.41
g. membrane	3	25	34	100	1.41
m. sheath outer	4	5	45	0	1.41
Follicle capsule	5	500	56	100	14.1
Animal head	6	∞	35	0.05	0.1

Left, i is subscript used to denote each mass, m is in µg. *Right*, ij is the subscript of an interaction between masses i and j, k is in kNm^{-1}, d is in $\mathrm{Nm}^{-1}\mathrm{s}$

is governed by two equations, one for each dimension, of the form

$$m_i l_{ij} \ddot{s}_{i,n} = \sum_j \left(k_{ij} \left(l_{ij} s_{j,n} - s_{i,n} \right) + d_{ij} \left(l_{ij} \dot{s}_{j,n} - \dot{s}_{i,n} \right) \right) \tag{1}$$

where m_i is the mass of the ith mass, k_{ij}, d_{ij} and l_{ij} are the spring, damper and lever constants reflecting the effect of the jth mass on the ith, and the (double-)dot notation denotes (double-)derivative against time. Note that $k_{ij} = k_{ji}$, $d_{ij} = d_{ji}$, but $l_{ij} = 1/l_{ji}$. Dependent on stimulus protocol, the stimulus contact point or the follicle capsule can be driven

$$s_{i,n} = g_n \tag{2}$$

with g_n some driving profile, in which case Eq. 1 is not computed for that mass. Alternatively, these masses can be constrained after computation of Eq. 1 to fall inside some finite

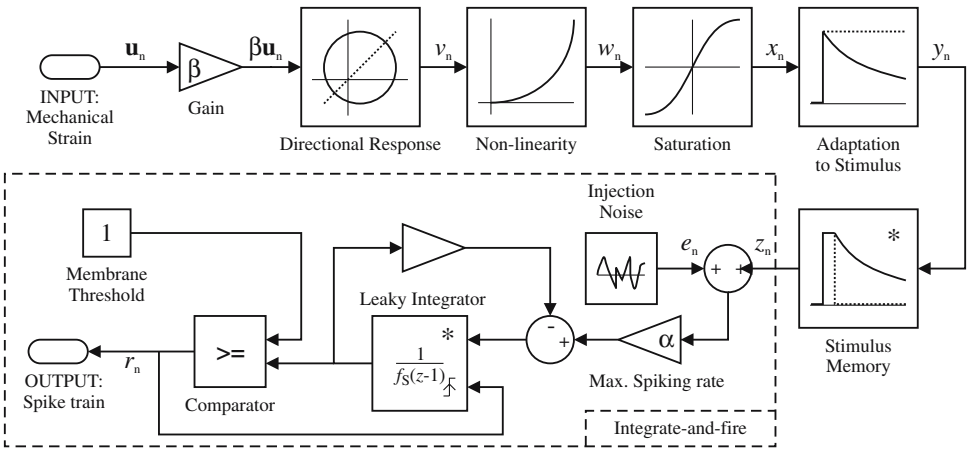

Fig. 3 Primary afferent part of model. Pre-processing stages are shown above and to the *right*, driving a standard noisy integrate-and-fire model enclosed in the *dashed region*. Items marked with an *asterisk* (stimulus memory and reset integrator) are modified herein beyond parameter changes

region (this is used to simulate obstruction of the whisker contact point by an obstacle). The parameters of the mechanical model are given in Table 1 (see the original modelling work for their derivation); all spring and damper constants not given are zero (see Fig. 2). The lever constants l_{ij} are unity for all i and j, except for the two values governing the interaction through the whisker shaft, which pivots within the follicle capsule: specifically, $l_{12} = -\sqrt{h}/0.27$, where h is the distance between the stimulus contact point and the facial skin (defined by the stimulus protocol). Because this lever representation encompasses the fact that the lever itself (the whisker) forms the interactions between masses m_1 and m_2, the lever constant also appears in the left hand side of Eq. 1 where it corrects for the change in stiffness of the whisker with its length.

Inputs to the mechanical model are drives or constraints of masses m_1 and/or m_5, as described above. Outputs are the strains $\mathbf{u}_{ij} = [u^1_{ij}, u^2_{ij}]$ in layers between mass components. Specifically, in the root and mesenchymal sheaths, $\mathbf{u}_{23}$ and $\mathbf{u}_{34}$, these being the locations of the mechanoreceptors presumed to serve the primary afferents. Each strain is given by two equations, one for each dimension, of the form

$$u_{ij,n} = \left(s_{j,n} - s_{i,n}\right)/b_{ij} \tag{3}$$

with b_{ij} the width of the layer; $b_{23} = 80\,\mu\text{m}$ and $b_{34} = 20\,\mu\text{m}$. Thus, diverse stimulation protocols can be simulated; we do not modify the mechanical model here.

These strains form the input to the electrical part of the model, representing the responses of primary afferents. The strains drive multiple parameterised instantiations of our primary afferent model, which is a noisy integrate-and-fire cell model (Eliasmith and Anderson 2003), preceded by several pre-processing stages implementing measured aspects of cell responses, Fig. 3. These stages represent the gain, directional response, non-linearity, saturation, adaptation, and stimulus 'memory' of each individual cell; they are governed by the following equations.

We hereby drop the subscript ij for notational simplicity. The directional response is then written as

$$v_n = 0.5\beta|\mathbf{u}_n|\left(\sqrt{b^2 - 4c} - b\right) \tag{4}$$

$$b = -\zeta\cos(\arctan(u^2_n/u^1_n) - \theta) \tag{5}$$

$$c = (\zeta/2)^2 - (1 - \zeta/2)^2 \tag{6}$$

This defines a circular function with gain β at the maximally effective angle (MEA) $\theta \in [0, 2\pi)$, and gain $\beta(1-\zeta)$ opposite the MEA, $\zeta \in [0, 1]$. The non-linearity is $w_n = v_n^\gamma$, with γ a parameter, and saturation $x_n = \tanh(w_n)$ caps the cell firing rate. Adaptation to stimulus was modelled as

$$y_n = x_n - q_n \tag{7}$$

$$q_n = (1 - \lambda_\text{A})x_n + \lambda_\text{A} q_{n-1} \tag{8}$$

with $\lambda_\text{A} = \exp(-1/(\tau_\text{A} f_S))$, and τ_A the adaptation time constant. y_n, thus, closely follows features in x_n with duration much less than τ_A, but responds decreasingly to features with longer durations. Stimulus memory was modelled as

$$z_n = \begin{cases} y_n, & y_n > \lambda_\text{M} z_{n-1} \\ \lambda_\text{M} z_{n-1}, & \text{otherwise} \end{cases} \tag{9}$$

with $\lambda_\text{M} = \exp(-1/(\tau_\text{M} f_S))$, and τ_M the memory time constant. The resulting 'response strength', z_n, forms the input of the integrate-and-fire cell model which generates the spike train

$$a'_n = \lambda_\text{D} a_n + \alpha\,(z_n + e_n) \tag{10}$$

$$r_{n+L} = \begin{cases} 0, & a'_n < 1 \\ 1, & \text{otherwise} \end{cases} \tag{11}$$

$$a_n = \begin{cases} a'_n, & a'_n < 1 \\ 0, & \text{otherwise} \end{cases} \tag{12}$$

with $\lambda_\text{D} = \exp(-1/(\tau_\text{D} f_S))$, τ_D the membrane time constant, $e_n \sim N(\mu, \sigma^2)$ additive membrane noise, α the maximum firing rate, $L = \tau_\text{L} f_S$, and τ_L the output delay which simulates generation and propagation latency. a_n is the membrane state, and r_n is the spike train at the output of the cell.

Table 2 Parameters of the nominal RA cell, and progressive models of Zurvan during the hand-tuning process

Model	nom.	Z1	Z2	Z3	Z4
τ_D(ms)	10	.	.	.	3.0
α	2000	.	.	.	.
μ	0.03	.	.	.	0.15
σ	0.1	.	.	.	.
ζ	0.6	.	1.0	.	.
γ	2	.	.	.	.
τ_A(ms)	5.0	.	.	.	.
τ_M(ms)	5.0	.	0.0	.	.
τ_R(ms)				1.5	.
V_R					−0.6
MEA		$-\pi/4$	.	.	.
τ_L(ms)	3.0	1.0	1.2	1.1	1.4
β	61.5	30	120	250	120

Dots indicate that this parameter is unchanged (so look left for its value). Empty indicates that this parameter is not applicable to this model

The parameters of a nominal RA cell from the existing model are given in the first column of Table 2.

Arabzadeh et al. (2005) used a recording protocol as follows. In one set of urethane-anaesthetised rats, whisking was artificially induced (through electrical stimulation of the facial nerve) whilst six different stimuli were presented to one intact whisker (free-space and five textured surfaces). Meanwhile, the two-dimensional movement of the whisker base (1 mm from skin) was recorded using an optical sensor, providing a set of whisker base movements that presumably are within the set that the rat would naturally encounter during normal behaviour. In an independent set of urethane-anaesthetised rats, recordings were made of single primary afferent cells whilst these pre-recorded stimuli were played back to a single whisker stub at 1 mm from the skin using a piezo-electric actuator. First, these stimuli were repeated as recorded, with each 'whisk' different. Next, a single stimulus consisting of four free whisks followed by four whisks against a texture was repeated identically multiple times, so that for each application the stimulus was as identical as the actuator would allow. Thereafter, for each cell, a long pseudo-random white Gaussian noise signal was presented at the actuator whilst recording continued. In both cases, signals were band-limited to 500 Hz before presentation to the actuator, to accommodate its response limits. We will refer to these two protocols, and the associated data sets, as 'natural' and 'noise', respectively. Note that, in contrast to responses in brainstem and above, responses in primary afferents are not observed to vary with anaesthetic level.

The natural data is the important set to fit, since it consists of primary afferent cells encoding ecologically relevant stimuli. The noise data, however, are useful for fitting models. In the absence of a parametric model, this type of noise is a good choice of input perturbation for system identification, at least for open-loop systems such as this, and provided the signal sequence is sufficiently long (600 s, here) (Godfrey 1993). We therefore fit the model using the noise data and test the result on the natural data. We fit and test a model of a single recorded cell; thus, we intend to prove the principle that first-order neuron responses can be explained by simple feed-forward models. This model will not describe all similar cells, but we speculate that parameter adjustment may allow it to reproduce the behaviour of some fraction. The cell we choose is that named 'Zurvan' in the original work, since its properties are thoroughly described therein, and its performance was precise and reliable.

2 Methods

We simulated the stimulation protocol of Arabzadeh et al. (2005), with whisker deflection delivered at 1 mm from the skin by a perfect actuator. To measure performance on the noise sequence, we compared model spike trains with those generated by Zurvan. To illustrate this analysis and at the same time analyse the statistical structure of the real cell data, we postulate a 'model' of the cell, Z0, which consists of the spikes recorded from Zurvan itself (i.e. Z0 is not really a model, but is identical to Zurvan). The analysis we will apply to the real models is illustrated using Z0 in the left half of Fig. 4. First, we compute the normalised histogram of inter-spike-intervals (ISI) of the model spike train (upper panel). The ISI plot for Z0 shows some periodicity, reflecting periodicity in the stimulus, and an absolute refractory period. We then compute the normalised cross-correlogram (or *conditional rate* function) of the model and Zurvan spike trains for visual comparison (Rieke et al. 1999) (middle panel, light grey). That for Z0 against Zurvan reflects the Zurvan ISI and settles at long offsets to a value reflecting the mean firing rate, 114 Hz. Next, for each spike in the recorded train we find the time offset to the nearest spike in the model train, and plot the histogram of these offsets as for the cross-correlogram (middle panel, dark grey); by analogy with the inter-spike-interval, we label this metric the 'inter-train-interval' (ITI). For the illustrative model, the ITI is a delta function.

The ITI facilitates a quantitative metric of train similarity: we count model spikes that fall within some time interval Δt of a recorded spike, and divide this count by the larger of the total number of spikes in each train, denoting this value $S_{\Delta t}$. This metric equals unity for trains that are identical within Δt (as shown), and approaches zero for increasingly dissimilar trains. For comparison, a model of Zurvan consisting of Zurvan spikes time-shifted by one second (same firing statistics, but presumably entirely uncorrelated with Zurvan spikes) returns $S_{0.5} = 0.12$. Retrospectively, we set the latency τ_L

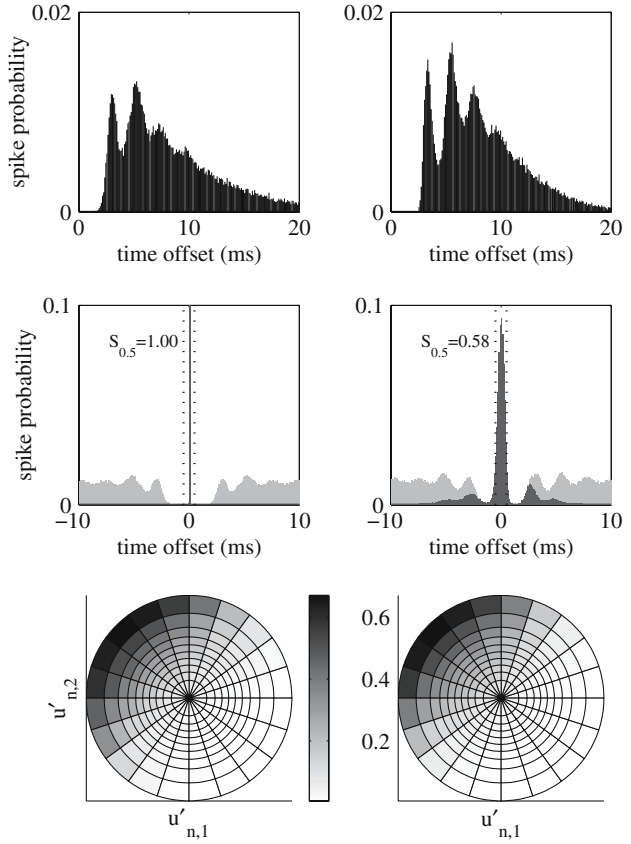

Fig. 4 Zurvan (*left*) and Z4 (*right*) as models of Zurvan. (*Upper*) Model ISI histograms. (*Middle*) Cross-correlograms (*light grey*) with ITI (test set) overlaid (*dark grey*); *dotted lines* indicate bounds of $S_{\Delta t}$. (*Lower*) Response probability profiles of models, u' denotes derivative of u

to maximise $S_{0.5}$. All these histograms use a bin width of 0.1 ms. Finally, we compute the stimulus-response *forward correlation* measure used in Arabzadeh et al. (2005) for the model (lower panel): for each of a discrete set of velocities of the stimulus, we compute the probability of a model spike occurring in the window 1–2 ms after the velocity feature, and construct a *response probability profile*, analogous to Fig. 10C of that work.

The response probability profile of Z0 (Fig. 4, lower left) shows that Zurvan responded most strongly to deflection velocities at an angle of approximately $3\pi/4$. Additionally, it did not respond during the plateau phase of a step deflection, so we concluded that it was a rapidly-adapting (RA) cell. Thus, our initial model of Zurvan, 'Z1', was an RA cell with parameters as described in Mitchinson et al. (2004), MEA set to $-\pi/4$ (the apparent MEA with respect to whisker stimulation will be as desired, since the whisker shaft lever flips the sense of the stimulus). The cell is driven by the strain in the mesenchymal sheath, $\mathbf{u}_{34}$, since this is purported to be the location of mechanoreceptors that drive RA afferents. Full analyses of interim models (Z1–Z3) of the hand-tuning are not shown to save space.

We made three approaches to model fitting. In each case, we used the performance ($S_{0.5}$) on one tenth of the noise data (60 s, 'test' set) as a metric to fit a model and the response to the natural data as a view on the performance of the model in response to ethologically relevant stimuli. The final model, identified after completing all three approaches, was validated through its response to the remaining noise data (540 s, 'validation' set). We only modified the primary afferent model in each approach, making no changes to the mechanical model. At each parameter space point in each approach, we adjusted the gain of the primary afferent model (β) so that the model average firing rate matched as closely as possible that of the recorded cell, before calculating $S_{0.5}$.

Our first approach was to hand-tune a model through four iterations (Z1–Z4), introducing additional structural features. A hand-tuning iteration was as follows. First, we analysed the performance of the current model on the first tenth of the noise data. Second, we postulated the parameter or structure changes that would improve performance. Third, new parameters were obtained by regular grid search in the space of each adjusted parameter to optimise performance on that data. Our second approach was to perform automatic unconstrained optimisation against all the non-mechanical parameters of the resulting cell model using a standard algorithm (MATLAB, fmincon) with multiple random starting points. Finally, we performed an exhaustive grid-search within the non-mechanical parameter space (with, by computational necessity, a lower resolution than the searches used during hand-tuning). These approaches are complementary: hand-tuning allows rapid progress and the incorporation of investigator experience into the tuning process; automatic optimisation is potentially rapid and effective if the problem is well-formed; exhaustive search is computationally intensive so cannot achieve the high resolution of exploration of the other approaches, but goes some way to ensuring that no region of parameter space is ignored overall.

3 Results

3.1 Fitting using noise data

The full parameter set of the unmodified model Z1 is reproduced in Table 2, along with the parameters of all subsequent models. The ISI histogram for Z1 looks like a smoothed version of that of Zurvan, but a broad cross-correlogram and $S_{0.5} = 0.2$ indicates that spike-timing performance is poor. This is expected, since this model was tuned against response profiles only, so whilst the statistics of the response were captured, the fine structure of spike-timing was not. Presented with the natural dataset, Z1 produces bursts of spikes in response to transient features, which can be traced to the model memory. Zurvan produces only single spikes

in response to these same features, indicating no measurable memory, so we drop the memory function entirely for the next model, Z2, by setting $\tau_M = 0$. Furthermore, the forward correlation analysis of Zurvan's response to the noise data indicates that it has very little response to stimuli with velocity vectors in the half-plane opposite its MEA, i.e. that it approaches perfect directional tuning. Z1 displays some considerable response to such stimuli both in the noise and natural data sets, revealing that it is less well directionally tuned. Thus, we set the directional tuning parameter of model Z2 to $\zeta = 1.0$ (perfect directional tuning). This latter change is not a change to the model in general—cells with widely ranging directional tuning are reported—but does highlight that RA cells can be as highly tuned directionally as SA cells.

Z2 clearly displays the periodicity present in the Zurvan ISI, and $S_{0.5}$ reaches 0.35. Furthermore, velocity vectors in the half-plane centred on $-\pi/4$ generate only around one percent of the spikes, (six percent for Zurvan itself), indicating similarly sharp directional tuning. There is, however, a very pronounced peak in the model ISI at a latency of under a millisecond, that is entirely missing in Zurvan; Zurvan cannot fire this fast (or, at least, does not under these conditions). As observed above, there is a marked minimum ISI for Zurvan of around 1.5 ms—we thus introduce an absolute refractory period to the model, $\tau_R = 1.5$ ms, during which period the membrane dynamics are not computed (a_n is held at zero), to form model Z3.

The very short ISI peak is eliminated, but short ISIs of around 3 ms are much too frequent—Zurvan produces more ISIs in its ISI peak around 6 ms than in that around 3 ms, indicating relative refractory behaviour. Aiming to reproduce this behaviour, we use a conventional technique to introduce a relative refractory period (Trappenberg 2002), resetting a_n to a negative value, V_R, instead of to zero, after the absolute refractory period (also limiting the membrane at the lower end to V_R). After obtaining V_R, we find that this change has an overly strong effect at longer intervals. The duration of influence of this relative refractory model is determined by the time constant of the integration membrane; therefore, we drop the membrane time constant τ_D to 3 ms to reduce this duration. In turn, this compromises the linearity of the membrane, so we retune it, raising the value of the constant injection current, μ, until linearity is approximately recovered. The performance of the resulting model, Z4, is shown in the right half of Fig. 4. The ISI and response probability profile are now good visual matches for those of Zurvan, and the ITI plot and $S_{0.5} = 0.58$ over the test set show much improvement. $S_{0.5} = 0.57$ over the validation set confirms that the model is not overfitted.

Automatic search was not able to improve on the hand-tuned model, either starting from the tuned model or starting from random points in parameter space (best models $S_{0.5} \approx 0.5$). In addition to $S_{\Delta t}$, we tried using D^{spike} (Victor and Purpura 1997) and smoothed variations of both of these as cost functions. Exhaustive grid search was more successful, returning a cell model with comparable performance to the hand-tuning, but the model found was essentially the same as that found through hand-tuning. We, therefore, did not replace the hand-tuned model.

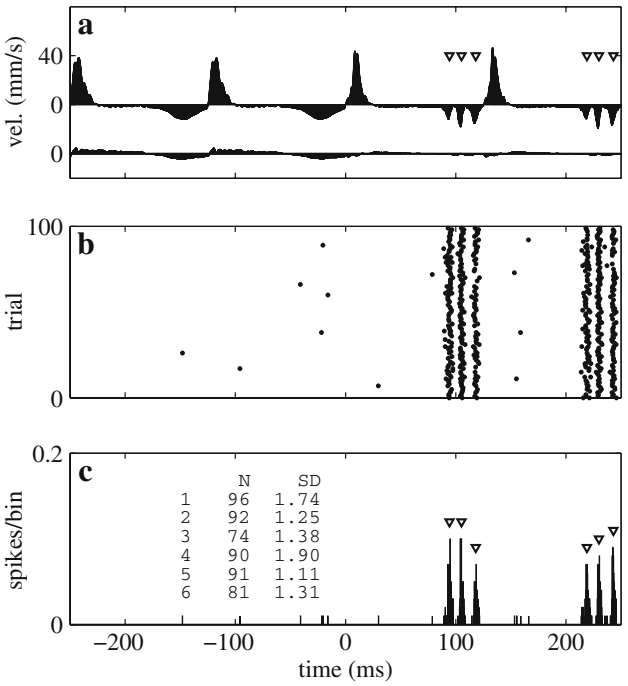

Fig. 5 Response of Z4 to the natural data for P280 texture, 100 different stimuli. **a** Average stimulus velocity profile showing two free whisks followed by two whisks against the texture, **b** response raster plot, **c** response PSTH. *Arrowheads* indicate velocity features to which Zurvan responded **a** and Z4 response peaks **c**. Figures in *lower panel* indicate total spikes (N) over all trials in response to each feature, and standard deviation in spike time of these (SD), with features labelled 1–6 in chronological order

3.2 Testing using natural data

We then present the natural dataset to Z4, both the multiple unique stimuli and the multiple repetitions of a single stimulus. The outputs of the model in response to each of these sets are shown in Figs. 5 and 6, respectively. The outputs of the biological cells in response to the same stimuli are available for comparison as panels a–c of Figs. 2 and 8, respectively, in the original work. The model outputs are similar for each stimulus set, corresponding closely to the responses of Zurvan. Z4 responds with approximately one spike to each of the main velocity features to which Zurvan responds; specifically, with a mean of 0.87 spikes/feature to the different stimuli, and with 0.99 spikes/feature to the identical stimuli set. The standard deviation (SD) of Z4 spike times in response to the identical stimuli is sensitive to the sharpness of the driving feature, but for four of the six features it is

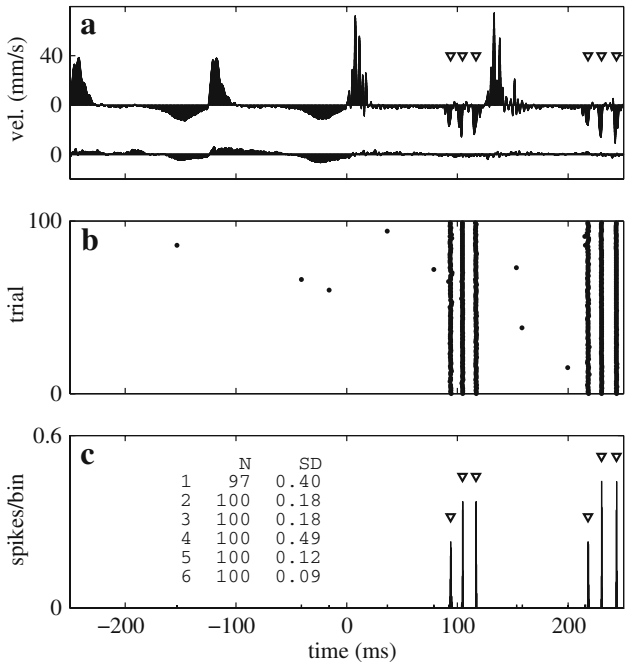

Fig. 6 Response of Z4 to the natural data for P280 texture, 100 identical stimuli. See figure above for details, except (**a**) repeated velocity profile

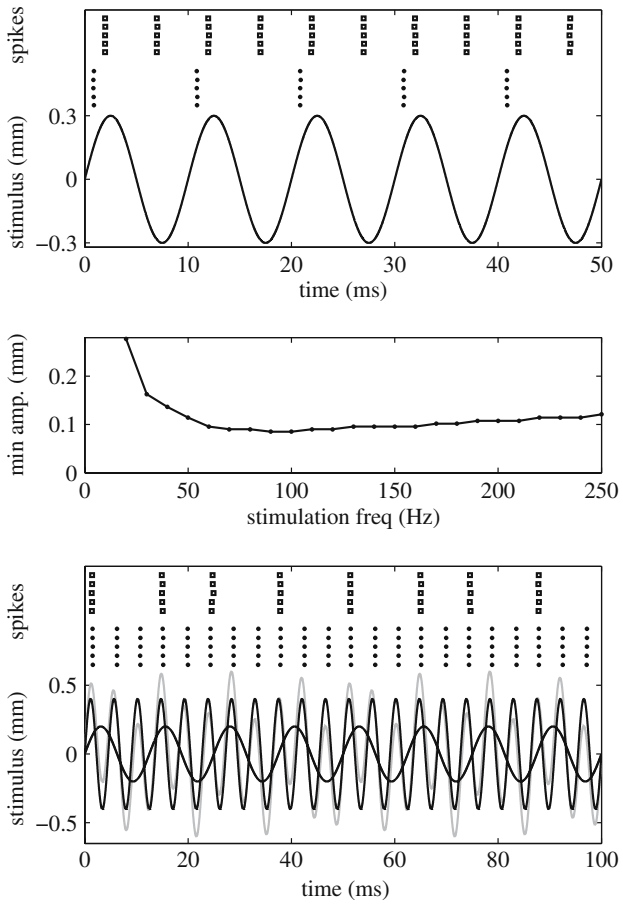

Fig. 7 (*Upper*) Oscillatory stimulus applied to model cells (*solid*), alongside rasters of responses of Z4 (*dots*) and Z4 without directional sensitivity (*squares*). (*Middle*) Tuning curve for Z4. (*Lower*) Composite oscillatory stimulus (*grey*) built from two sinusoidal signals (*black*), alongside rasters of responses of two Z4-similar cells with different gains

in 0.08–0.17 ms, which is comparable to that of Zurvan (∼0.1 ms). The variability in response time to the multiple stimuli set is comparable to that of Zurvan, reflecting that the main source of variability here is the stimulus itself.

For both sets, there is a small amount of response away from the most prominent velocity features, but it is not very marked. This is in reasonable qualitative agreement with results from Zurvan, though Zurvan has a substantially stronger response to retraction during free whisking. These less prominent responses may carry information, and are effectively not reproduced by the model, but they constitute less than 10% of the total response of the cell. Overall, the match between Z4 and Zurvan is visually impressive.

3.3 Testing with oscillatory data

Another common observation in somatosensory peripheral encoding studies is the ability of a cell to reliably report the phase of an oscillatory stimulus (*phase-locking*), and to show a frequency-dependent response. This has been reported in several species including Rat (Hahn 1971; Gottschaldt et al. 1973; Gottschaldt and Vahle-Hinz 1981; Freeman and Johnson 1982; Gibson and Welker 1983b), but could not be reproduced by our previous model since high-frequency responses were largely eliminated by the memory component. We presented a 100 Hz sine-wave stimulus to Z4 along the MEA, and the resulting spike trains over five realisations are presented in the upper panel of Fig. 7. Z4, without memory, displays reliable phase-locking, always firing during the positive-going swing of the stimulus. Some biological cells respond to both swings of such stimuli: we repeated five realisations setting Z4's directional sensitivity to zero, and report the results in the same figure. This alternative model cell responds, as expected, to swings of both polarities. Higher amplitude stimuli can elicit multiple spikes per swing from Z4, as seen in biological data. In general, Z4 displays *s* spikes per period, with *s* usually some integer or reciprocal integer dependent on stimulus amplitude and frequency. In the middle panel of Fig. 7 we present the *tuning curve* of the model for sinusoidal stimuli: for each frequency, we plot the minimum amplitude at which Z4 first exhibits one spike per cycle of the stimulus (above 250 Hz the minimum amplitude quickly shoots up until one spike per cycle cannot be achieved). This plot is analogous to, and has the same form as, those in (Hahn 1971; Gottschaldt et al. 1973), for example. Recent results (Neimark et al. 2003; Hartmann et al. 2003; Kim and Möller 2004) suggest that natural tactile information may contain

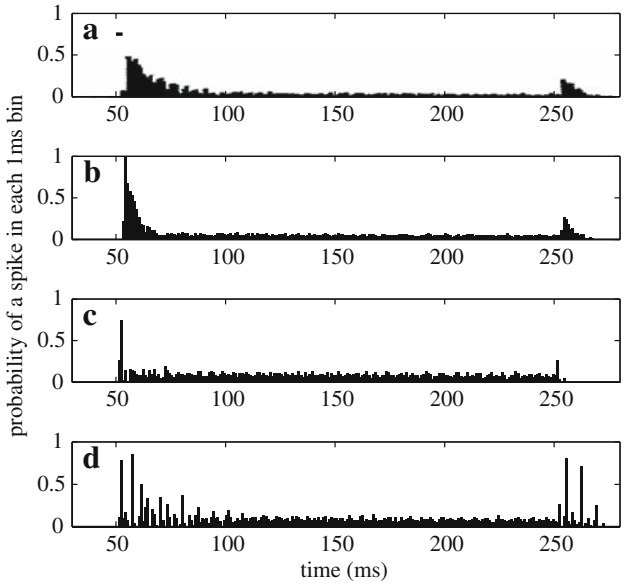

Fig. 8 **a** Reproduction of population response histogram for ramp-hold-release stimulus with 3 ms rise time, from Shoykhet et al. (2000), *upper left panel* of Fig. 1 in that work—short floating bar at 50 ms indicates duration of 3 ms stimulus ramp. Simulation of that protocol driving model cells produces results: **b** original follicle model, **c** original follicle model with memory component removed, and **d** as **c** but with actuator ringing modelled by stimulus filtering (see text for details)

information at multiple frequencies. In the lower panel of Fig. 7 we illustrate how two Z4-similar cells (Z4 with appropriately chosen gain, β) can extract and encode the individual components of a composite stimulus containing signals at 80 and 220 Hz reliably over five realisations. Such responses could form the basis of distributed encoding in the frequency domain.

3.4 Memory and mechanical ringing

Figure 8a gives the population response of 81 SA and RA cells recorded in the rat trigeminal ganglion to a ramp-and-hold stimulus, from Shoykhet et al. (2000). This illustrates the effect that was described by the memory component of the original model—the 3 ms rise ramp of the stimulus (indicated by solid bar) elicits a 30–40 ms response—and the response of the original model to the same stimulus is given in Fig. 8b. This response does not represent adaptation in some cells, since individual cells typically exhibit very long or short time constants of adaptation whilst still displaying this medium-term response to some transient stimuli (Lichtenstein et al. 1990; Kyriazi et al. 1994; Jones et al. 2004). However, no cell studied by Arabzadeh et al. (2005) was found to display memory (personal communication). In light of this, we now believe that this effect is not a general characteristic of ganglion cells. Removing the memory effect in the model and repeating the simulation of Fig. 8b gives results as shown in Fig. 8c, with a truncated transient response to stimulus onset and offset.

The apparent memory may instead be attributable to some feature of stimulus delivery to the mechanoreceptors, that is, mechanical ringing (Robichaud et al. 2003) in some component. Ringing has been observed in the type of actuators used for primary afferent studies (Simons 1983), though stimulus pre-filtering has typically been used to reduce or eliminate it. It has also been observed in intact whiskers (Hartmann et al. 2003; Mehta and Kleinfeld 2004; Andermann et al. 2004), though we are not aware that it has been assessed in trimmed whiskers. Both sources have appropriate time profiles to cause the observed responses; ringing in the internal components of the follicle seems less likely, because we expect it to be too short-lived. Some filter designs can also have similar effects (Robichaud et al. 2003)—the Bessel filter suggested in Simons (1983) does not, but that filter cannot be used with high velocity stimuli, and the filtering used in all other studies is unreported.

We cannot say which of these sources leads to the memory usually observed, but we demonstrate, here, that mechanical ringing can reproduce it. We repeat the experiment of Fig. 8c, using the ramp-and-hold stimulus, g'_n, to drive an underdamped second-order oscillator

$$\ddot{g}_n = \omega_0^2(g'_n - g_n) + 2\zeta\omega_0(\dot{g}'_n - \dot{g}_n) \tag{13}$$

(natural frequency $\omega_0 = 600\pi\,\mathrm{Rs}^{-1}$ and damping constant $\zeta = 0.05$) and using the response of this oscillator to drive the memoryless model. The result, in Fig. 8d, shows the effective prolonging of the transient responses. Whilst the response periodicity introduced is not apparent in biological population responses (e.g. panel A), it is apparent in histograms constructed from multiple trials with single biological cells (Lichtenstein et al. 1990; Kyriazi et al. 1994; Jones et al. 2004; Minnery and Simons 2003).

4 Discussion

The RA afferent model previously published (Z1) was based on statistical response profiles, probably obfuscated by convolution with actuator response, or with more complex whisker response than was modelled, and was not a good model of a particular cell, Zurvan, at a spike-timing level. However, removing the memory component and implementing a more realistic membrane model with refractory effects resulted in a marked performance improvement, and we have justified these changes. The resulting model, Z4, matches almost two thirds of Zurvan spikes in response to a noise stimulus with an accuracy of 0.5 ms or better (better than two-thirds for an accuracy of 1.0 ms), as opposed to a model not driven by the stimulus but with the same firing statistics

(outlined in Sect. 2) which matches only 12% of spikes to this accuracy. Furthermore, both the firing statistics (indicated by the ISI histogram) and the velocity response profile (polar plot) are good visual matches for those of the real cell. We have, additionally, demonstrated that this new model produces responses to naturalistic stimuli that are almost identical to those produced by Zurvan. Finally, we have shown that the model can phase-lock to oscillatory stimuli and produces a natural-looking tuning curve, and demonstrated that multiple (2, here) instantiations of this model can extract and encode individual frequency components of a composite periodic signal, a distributed encoding that is often implied for biological sensory cells.

How 'good' is this model performance in real terms? We do not have cell response data to multiple presentations of the noise stimulus, but responses to multiple presentations of identical natural data suggest that Zurvan can achieve excellent (approaching 100%) spike-for-spike matching between presentations (for spikes in response to 'features' of the stimulus), with timing jitter standard deviation ~0.1–0.2 ms. This is superior to the match between Zurvan and Z4 as shown by the noise data—finding all the spikes that are 'shared' between Zurvan and Z4 in response to the noise data by choosing only those that fall within 0.5 ms of each other, and computing the timing jitter of only these spikes, gives 58% shared spikes with a jitter standard deviation of 0.23 ms. However, the response of Z4 to the identical natural data shows it to be comparable in reliability to Zurvan in this context, with average 99% spike-for-spike matching and timing jitter standard deviation in the 0.1–0.2 ms range for 4 of 6 features.

We might argue that a real or simulated cell cannot usefully encode information at these very high levels of precision, because the noise introduced by variability between samplings of the stimulus (e.g. sandpaper) swamps the intrinsic timing jitter of the cell (timing variability from Zurvan using non-identical stimuli was nearer 1 ms). However, this argument requires an assumption that is unlikely to hold—that noise introduced from variability of whisker motion at Zurvan is uncorrelated with noise introduced due to the same variability at Zurvan's sister cells. This assumption might be tested by recording from multiple ganglion cells simultaneously under a multiple non-identical stimulus battery, and comparing intra- and inter-trial correlations between cell responses. Given the very high stimulus reproducibility that is evident from the very high response reproducibility shown in Arabzadeh et al. (2005), it is probably safe to relax the requirement for simultaneous recording.

In summary, we have demonstrated a simple electromechanical model that can reproduce much of the behaviour of a particular rapidly adapting primary afferent cell from the rat trigeminal ganglion at a spike-timing scale. This does not constitute a general transduction model, but high performance at this scale furthers our approach towards a broadly applicable model of somatosensory transduction in whiskered animals. In future, we intend to generalise this model by obtaining and fitting data from cells with a variety of response classes through further iterative model improvements. The model is currently in use both in hardware and in simulation, transducing signals from artificial whiskers as a component of an artificial whisker sensorimotor system, as part of our continuing work towards a complete model of vibrissal guidance of rat behaviour (Mitchinson et al. 2006; Pearson et al. 2007). We believe that accurately describing peripheral encoding should be prioritised by workers wishing to understand the function of higher centres in sensory pathways and cortical sensory processing.

We are grateful to Erik Zorzin for help in collecting and presenting the texture stimulus set. We would also like to thank the anonymous reviewers for their helpful comments.

References

Ahissar E, Sosnik R, Haidarliu S (2000) Transformation from temporal to rate coding in a somatosensory thalamocortical pathway. Nature 406(6793):302–306

Andermann ML, Ritt J, Neimark MA, Moore CI (2004) Neural correlates of vibrissa resonance; band-pass and somatotopic representation of high-frequency stimuli. Neuron 42(3):451–463

Arabzadeh E, Zorzin E, Diamond ME (2005) Neuronal encoding of texture in the whisker sensory pathway. PLoS Biol 3(1):e17

Bensmaïa S (2002) A transduction model of the meissner corpuscle. Math Biosci 176(2):203–217

Bensmaïa SJ, Sripati A, Johnson KO (2005) A biophysical model of afferent responses to dynamic stimuli. Poster presented at the 35th annual meeting of the Society for Neuroscience, Washington, DC

Dykes RW (1975) Afferent fibers from mystacial vibrissae of cats and seals. J Neurophysiol 38(3):650–662

Ebara S, Kumamoto K, Matsuura T, Mazurkiewicz JE, Rice FL (2002) Similarities and differences in the innervation of mystacial vibrissal follicle-sinus complexes in the rat and cat: a confocal microscopic study. J Comp Neurol 449(2):103–119

Eliasmith C, Anderson CH (2003) Neural Engineering. MIT Press, Cambridge

Freeman AW, Johnson KO (1982) Cutaneous mechanoreceptors in macaque monkey: temporal discharge patterns evoked by vibration, and a receptor model. J Physiol 323:21–41

Gibson JM, Welker WI (1983a) Quantitative studies of stimulus coding in first-order vibrissa afferents of rats. 1. Receptive field properties and threshold distributions. Somatosens Res 1(1):51–67

Gibson JM, Welker WI (1983b) Quantitative studies of stimulus coding in first-order vibrissa afferents of rats. 2. Adaptation and coding of stimulus parameters. Somatosens Res 1(2):95–117

Godfrey K (ed) (1993) Perturbation signals for system identification. Prentice Hall, Englewood Cliffs

Gottschaldt KM, Iggo A, Young DW (1973) Functional characteristics of mechanoreceptors in sinus hair follicles of the cat. J Physiol 235(2):287–315

Gottschaldt KM, Vahle-Hinz C (1981) Merkel cell receptors: structure and transducer function. Science 214(4517):183–186

Hahn JF (1971) Stimulus-response relationships in first-order sensory fibres from cat vibrissae. J Physiol 213(1):215–226

Hartmann MJ, Johnson NJ, Towal RB, Assad C (2003) Mechanical characteristics of rat vibrissae: resonant frequencies and damping in isolated whiskers and in the awake behaving animal. J Neurosci 23(16):6510–6519

Jones LM, Lee S, Trageser JC, Simons DJ, Keller A (2004) Precise temporal responses in whisker trigeminal neurons. J Neurophysiol 92(1):665–668

Kim D, Möller R (2004) A biomimetic whisker for texture discrimination and distance estimation. In: Proc of the Int Conf on the Sim of Adap Behav (SAB)

Kleinfeld D, Ahissar E, Diamond ME (2006) Active sensation: insights from the rodent vibrissa sensorimotor system. Curr Opin Neurobiol 16(4):435–44

Kyriazi HT, Carvell GE, Simons DJ (1994) Off response transformations in the whisker/barrel system. J Neurophysiol 72(1):392–401

Kyriazi HT, Simons DJ (1993) Thalamocortical response transformations in simulated whisker barrels. J Neurosci 13(4):1601–1615

Lichtenstein SH, Carvell GE, Simons DJ (1990) Responses of rat trigeminal ganglion neurons to movements of vibrissae in different directions. Somatosens Mot Res 7(1):47–65

Ma PM (1991) The barrelettes–architectonic vibrissal representations in the brainstem trigeminal complex of the mouse. I. Normal structural organization. J Comp Neurol 309(2):161–199

Mehta SB, Kleinfeld D (2004) Frisking the whiskers. Patterned sensory input in the rat vibrissa system. Neuron 41(2):181–184

Minnery BS, Simons DJ (2003) Response properties of whisker-associated trigeminothalamic neurons in rat nucleus principalis. J Neurophysiol 89(1):40–56

Mitchinson B, Gurney KN, Redgrave P, Melhuish C, Pipe AG, Pearson M, Gilhespy I, Prescott TJ (2004) Empirically inspired simulated electro-mechanical model of the rat mystacial follicle-sinus complex. Proc R Soc Lond B Biol Sci 271(1556):2509–2516

Mitchinson B, Pearson M, Melhuish C, Prescott TJ (2006) A model of sensorimotor coordination in the rat whisker system. In: Proceedings of The International Conference on Simulation of Adaptive Behavior (ISAB)

Neimark MA, Andermann ML, Hopfield JJ, Moore CI (2003) Vibrissa resonance as a transduction mechanism for tactile encoding. J Neurosci 23(16):6499–6509

Pearson MJ, Pipe AG, Melhuish C, Prescott TJ (2007) Whiskerbot: a robotic active touch system modeled on the rat whisker sensory system. Adapt Behav 15:223–240

Pinto DJ, Brumberg JC, Simons DJ (2000) Circuit dynamics and coding strategies in rodent somatosensory cortex. J Neurophysiol 83(3):1158–1166

Rhodes PA, Llinás R (2005) A model of thalamocortical relay cells. J Physiol 565(Pt 3):765–781

Rice FL, Mance A, Munger BL (1986) A comparative light microscopic analysis of the sensory innervation of the mystacial pad. I. Innervation of vibrissal follicle-sinus complexes. J Comp Neurol 252(2):154–174

Rieke F, Warland D, Steveninck RDRV, Bialek W (1999) Spikes: exploring the neural code. MIT Press, Cambridge

Robichaud DR, Prete ZD, Grigg P (2003) Stretch sensitivity of cutaneous RA mechanoreceptors in rat hairy skin. J Neurophysiol 90(3):2065–2068

Shoykhet M, Doherty D, Simons DJ (2000) Coding of deflection velocity and amplitude by whisker primary afferent neurons: Implications for higher level processing. Somatosens Mot Res 17(2):171–180

Simons DJ (1983) Multi-whisker stimulation and its effects on vibrissa units in rat SmI barrel cortex. Brain Res 276:178–182

Slavík P, Bell J (1995) A mechanoreceptor model for rapidly and slowly adapting afferents subjected to periodic vibratory stimuli. Math Biosci 130(1):1–23

Szwed M, Bagdasarian K, Ahissar E (2003) Encoding of vibrissal active touch. Neuron 40(3):621–630

Trappenberg TP (2002) Fundamentals of computational neuroscience. Oxford University Press, Oxford

Van der Loos H (1976) Barreloids in mouse somatosensory thalamus. Neurosci Lett 2:1–6

Victor JD, Purpura KP (1997) Metric-space analysis of spike trains: theory, algorithms and application. Network 8:127–164

Waite PME (2004) Trigeminal sensory system. In: Paxinos G (ed) The rat nervous system. Elsevier, Amsterdam pp 817–851

Woolsey TA, Van der Loos H (1970) The structural organization of layer IV in the somatosensory region (SI) of mouse cerebral cortex. the description of a cortical field composed of discrete cytoarchitectonic units. Brain Res 17(2):205–242

Zucker E, Welker WI (1969) Coding of somatic sensory input by vibrissae neurons in the rat's trigeminal ganglion. Brain Res 12(1):138–156